Received: 7 April 2025 | Revised: 15 August 2025 | Accepted: 30 September 2025 | Published online: 24 October 2025

RESEARCH ARTICLE

Artificial Intelligence and Applications
2025, Vol. 00(00) 1-11
DOI: 10.47852/bonviewAIA52025860

BON VIEW PUBLISHING

Effective Denoising of Epileptic High-Frequency Oscillations (HFOs) in Scalp EEG Using a Temporal Generative Adversarial Network (TimeGAN)

Sahbi Chaibi[1,2,*], Wadhah Ayadi[3] and Abdennaceur Kachouri[1]

[1] *AFD2E Laboratory, Sfax University, Tunisia*

[2] *Faculty of Sciences, University of Monastir, Tunisia*

[3] *Laboratory of Electronics and Microelectronics, University of Monastir, Tunisia*

Abstract: Over the past two decades, High-Frequency Oscillations (HFOs) have been widely recognized as promising biomarkers for delineating the specific regions of the brain responsible for seizure onset, and for monitoring the spatiotemporal dynamics of epileptogenic activity. While deep learning (DL) techniques have shown promise in processing HFOs in intracranial EEG (iEEG) data, they often struggle to perform effectively on scalp electroencephalography (EEG). This limitation is particularly owing to the inherently lower signal-to-noise ratio of scalp HFOs, their smaller amplitude, and their increased susceptibility to artifact contamination, which together obscure subtle high-frequency phenomena. Despite these restrictions or barriers, clinicians predominantly rely on scalp EEG recordings due to their noninvasive nature, low cost, and recognized safety. To extend the benefits or applicability of DL-based HFO detection to a broader patient population, automated scalp EEG systems incorporating HFO denoising algorithms are highly warranted and necessary. Hence, the present study aimed at proposing, developing, and comparing the effectiveness of five optimized DL-based paradigms for denoising unwanted artifacts from realistic scalp EEG. The target data was created by combining intracranial HFO samples with injected realistic contaminants such as electrooculogram (EOG) and electromyography (EMG), accurately replicating scalp EEG profiles. In this regard, we considered evaluating and comparing the following time-series DL architectures, referred to as: one-dimensional Convolutional Neural Networks (CNN-1D), Long Short-Term Memory (LSTM) networks, Stacked Autoencoders (SAE), one-dimensional Transformer (Transformer-1D), and Generative Adversarial Networks (GAN). This analysis aims to elucidate each model's denoising performance strengths and weaknesses. The reached quantitative and qualitative experimental results revealed that the proposed current GAN model significantly achieved superior performance compared to other DL approaches, suggesting its effectiveness as a robust solution for denoising scalp HFOs, thereby enhancing noninvasive HFOs detection.

Keywords: epilepsy, EOG, EMG, HFOs, denoising, temporal GAN

1. Introduction and Literature Review

Epilepsy is a neurological disorder characterized by intermittent seizures resulting from abnormal or excessive neuronal activity in the brain. Recent research studies on HFOs have highlighted their remarkable potential as valuable spatial biomarkers for effectively localizing epileptogenic zones and tracking the underlying spatiotemporal dynamics of the epileptic networks [1, 2]. Research conducted on both human and animal models has established a noticeable association between HFOs and brain tissue capable of generating seizures [3]. HFOs could be invasively recorded via clinical iEEG emitted signals [4]. Other studies, however, maintained that HFOs might also be non-invasively captured via scalp EEG or magnetoencephalography (MEG) [5–7]. HFOs are characterized as spontaneous rhythmic oscillations with low amplitude and brief durations (30–100 ms), exhibiting at least three distinguishable cycles that clearly stand out from the background activity. Despite the HFOs' frequency range variations across studies, they are generally classified to range between 80 Hz and 500 Hz, including three major subtypes: High-Gamma (HG, 80–120 Hz), Ripples (Rs, 120–250 Hz), and Fast Ripples (FRs, 250–500 Hz) [8]. Pathological HFOs offer various clinical benefits in epilepsy and might serve as biomarkers for pre-surgical diagnosis and accurate localization of the Seizure Onset Zone (SOZ) in refractory epilepsy affected patients [9, 10]. In this regard, removing pathological HFO-producing tissue has been highly associated with improved surgical outcomes and higher rates of seizure freedom [2, 11]. Additionally, HFOs may act as important biomarkers for predicting seizures, thereby, enhancing the affected individuals' life quality [12]. Their detection during epilepsy surgery could significantly help in predicting surgical outcomes [13] and might also provide insights into the underlying seizure-generating properties of brain tissue [14]. More recently, a wide range of DL based algorithms have been developed to reduce reliance on HFOs' manual analysis, thus, mitigating human bias. In this respect, various state-of-the-arts deep learning (DL) algorithms have been developed, achieving impressive and promising results, and demonstrating remarkable performance in identifying pathological HFOs associated with

***Corresponding author:** Sahbi Chaibi, AFD2E Laboratory, Sfax University and Faculty of Sciences, University of Monastir, Tunisia. Email: sahbi.chaibi@fsm.rnu.tn

intracranial EEG. Nevertheless, most of the existing DL algorithms have been primarily developed to detect iEEG recorded invasive HFOs.

Still, clinical practice relies heavily on scalp EEG [8, 15], owing especially to its non-invasive nature, which has created a pressing and ongoing need to develop robust DL-based HFO detectors specifically tailored for processing scalp EEG data. In fact, scalp EEGs are more susceptible to persistent artifacts and physiological activity sources, resulting in reduced signal-to-noise ratios compared to iEEG, which obscures the subtle high-frequency phenomena [8, 16–18]. Current DL algorithms applied for processing iEEG recorded that invasive HFOs do not seem to perform effectively with scalp EEG cases [8, 17, 18]. Yet, detecting HFOs in scalp EEG is particularly challenging and considered as a complex process, owing to their low amplitude, brief duration, and very low signal-to-noise ratio. Such a contamination might well result in a high incidence of false HFO detections, emanating mainly form the interference of various sources, usually perceived in electroencephalographic (EEG) recordings, including electrooculographic (EOG) and electromyographic (EMG) artifacts, and less often, in cardiac artifacts (ECG). Removing or rejecting artifacts from scalp EEG is, therefore, crucial for an effective interpretation of EEG recordings, and their ultimate use in the form of HFOs spatiotemporal brain mapping [2, 19]. Yet, both EMG and EOG associated artifacts turn out to be too difficult to omit due to their high amplitude, variable topographical distribution, and widespread frequency. In effect, artifacts of various types share closely similar morphological characteristics with HFOs in both frequency and time domains. Separating HFO bursts from various artifact activities remains a major challenge within the invasive EEG (iEEG) domain and is even more difficult in the scalp EEG denoising field [20]. Currently, according to relevant literature, the most recently released state-of-the-art DL-based regression models dealing with electrophysiological data denoising, turn out to rely either on one-dimensional Conventional Neural Networks (CNN-1D) [15, 21–25], on Long Short-Term Memory (LSTM) [15], on Generative Adversarial Networks (GAN) [26–31], on one-dimensional Transformer (Transformer-1D) [15, 32, 33], or on Stacked Autoencoders (SAE) [34]. Regarding the present study, we undertook to propose, optimize, test, assess, and compare the performance potential of different denoising designs. Our main goal was to determine the most effective model fit for accurately removing noise from scalp EEG bearing contaminated HFO activities. The remainder of this paper is organized as follows. Following the introduction, Section 2 describes the intracranial EEG database, along with the scalp EEG artifact dataset used in this study. It also provides a brief overview of the preprocessing steps and methodologies employed, along with an introduction to the core DL paradigms explored and their respective key learning hyperparameters. This section concludes by presenting the EEG denoising evaluation metrics applied.

Subsequently, Section 3 presents the experimental results, introducing the proposed optimized DL architectures and their tuned hyperparameters, along with detailed assessments and comparisons of denoising performance. Section 4 is devoted to an in-depth discussion and comparison of the attained qualitative and quantitative results, while highlighting the contributions we have made as well as the main limitations of this research. The ultimate section presents the major conclusions achieved, along with a summary of the research findings and potential future directions.

2. Methods and Materials

Our proposed DL-based experimental framework for the automatic denoising of epileptic HFO patterns in scalp EEG signals involves several key steps: data collection, preprocessing, data splitting, model training, tuning and hyperparameter optimization of different implemented deep neural networks, and finally, the evaluation of the optimized models. Initially, intracranial EEG channels recorded from various electrode contacts located in epileptogenic regions were selected. Afterward, a thorough inspection was conducted by experienced clinicians to identify and label epileptic HFO events in our dataset. Subsequently, during the preprocessing phase, the annotated HFO samples were mixed with noise artifacts at varying signal-to-interference ratio (SIR) levels. After preprocessing, the data were subsequently divided into training, validation, and test sets. Each DL model was then trained on the prepared dataset, and its hyperparameters were carefully tuned to improve performance and achieve the best possible regression results. Finally, the models' effectiveness was evaluated using five widely used metrics, providing a comprehensive assessment of their predictive accuracy and reliability. Figure 1 below provides an overview of the proposed methodology, though the actual implementation may include additional steps or variations depending on the techniques and algorithms used in the study.

2.1. Dataset, visualizations and software environments

Two datasets were used in our experiments. The first was collected at the Montreal Neurological Institute and Hospital (MNI) in Canada. The second, denoted as EEGdenoiseNet, was sourced from [35]. Dataset 1 consists of intracranial EEG signals recorded from three patients suffering from refractory epilepsy. These signals were initially preprocessed using a low-pass anti-aliasing filter set at 500 Hz, followed by sampling at a rate of 2 kHz. The MNI dataset consists

Figure 1
Framework of the overall HFO denoising procedure using DL models

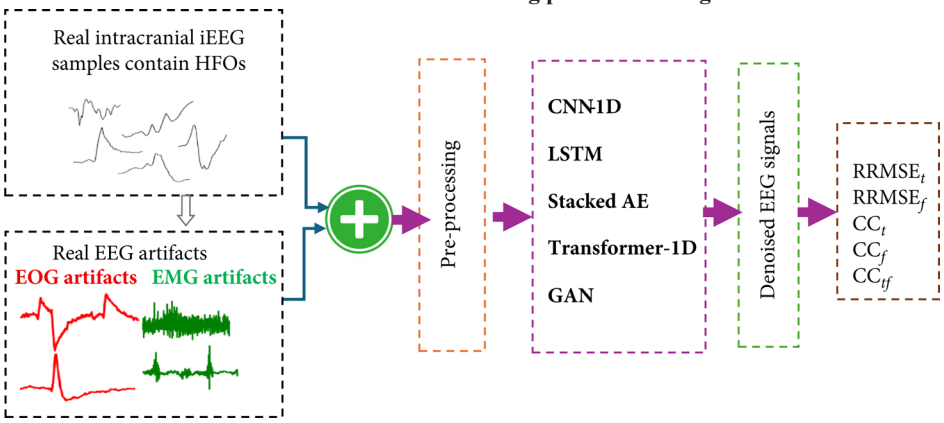

of recordings from 24 subdural grid channels and 70 depth sEEG channels, each lasting about 4 min. Recordings were obtained during interictal periods from bilateral mesial temporal lobe (MTL) structures. Data collection followed ethical guidelines, with all patients providing informed consent according to MNI research protocols. After review by experienced neurologists, 314 distinct HFO events were identified and retained for further analysis. These experts' visual annotations served as the gold-standard benchmark for optimizing and assessing the performance of DL models designed in this study. Figure 2 illustrates the graphical interface used to mark and inspect HFO samples.

Regarding the second noise source, we also used the widely adopted EEGdenoiseNet dataset [35], which serves as a benchmark for artifact denoising. It contains 3400 clean ocular artifact (EOG) samples and 5598 pure muscular artifact (EMG) signals, enabling the synthesis of contaminated EEG signals. Following previously renowned studies [21, 23, 24, 30, 32, 35], the signal-to-interference ratio (SIR) values appropriate for contaminating our iEEG HFO segments were set to range from −14 dB to 5 dB.

Although larger datasets, especially long EEG recordings from multiple subjects, are crucial for developing and training reliable deep neural network models, we believe that our dataset is of paramount importance for several reasons. Firstly, access to large clinical HFO datasets is frequently impeded by privacy concerns, consent issues, potential misuse, and institutional barriers. Nevertheless, despite these challenges, our limited dataset demonstrates the feasibility of leveraging DL for scalp HFO denoising.

Second, for proof-of-concept studies like ours, using a few hundred annotated HFO events as preliminary research enables testing the usefulness, applicability, and practicality of the proposed approaches. This serves as a foundational step toward developing more robust DL models in future work. Indeed, many successful DL models were initially trained on small datasets, with validation conducted on larger datasets during later development stages. Lastly, cross-validation helps mitigate the challenges posed by limited data size by enhancing the reliability and generalizability of the models. Specifically, in this study, various techniques, methodologies, and experimental simulations were implemented using the Anaconda Python environment, MATLAB, and the Google Colab cloud platform.

2.2. Data preprocessing

Preprocessing EEG data is a crucial step to improve data quality and facilitate meaningful analysis. According to our research objectives, the basic initial preprocessing steps include normalization, resizing or rescaling samples, adding noise, and mixing. Max-Abs normalization was applied to ensure that the models received consistent input, thereby enhancing training effectiveness and convergence. This method scales the dataset values to a specific range, between −1 and 1, bringing all data onto a comparable scale. While EEGdenoiseNet [35] includes 3400 eye artifact (EOG) and 5598 muscle artifact (EMG) sequences, each containing 512 samples after our adjustments, each labeled HFO event was also resized to 512 samples to match the EEGdenoiseNet segment length. Additionally, the EEGdenoiseNet artifact dataset was resampled to 2000 Hz to ensure all datasets shared the same sampling frequency. With respect to our study, EEGdenoiseNet is used as a publicly available benchmark dataset widely adopted by the research

Figure 2
A snapshot of the graphical user interface (GUI) used for HFO annotation

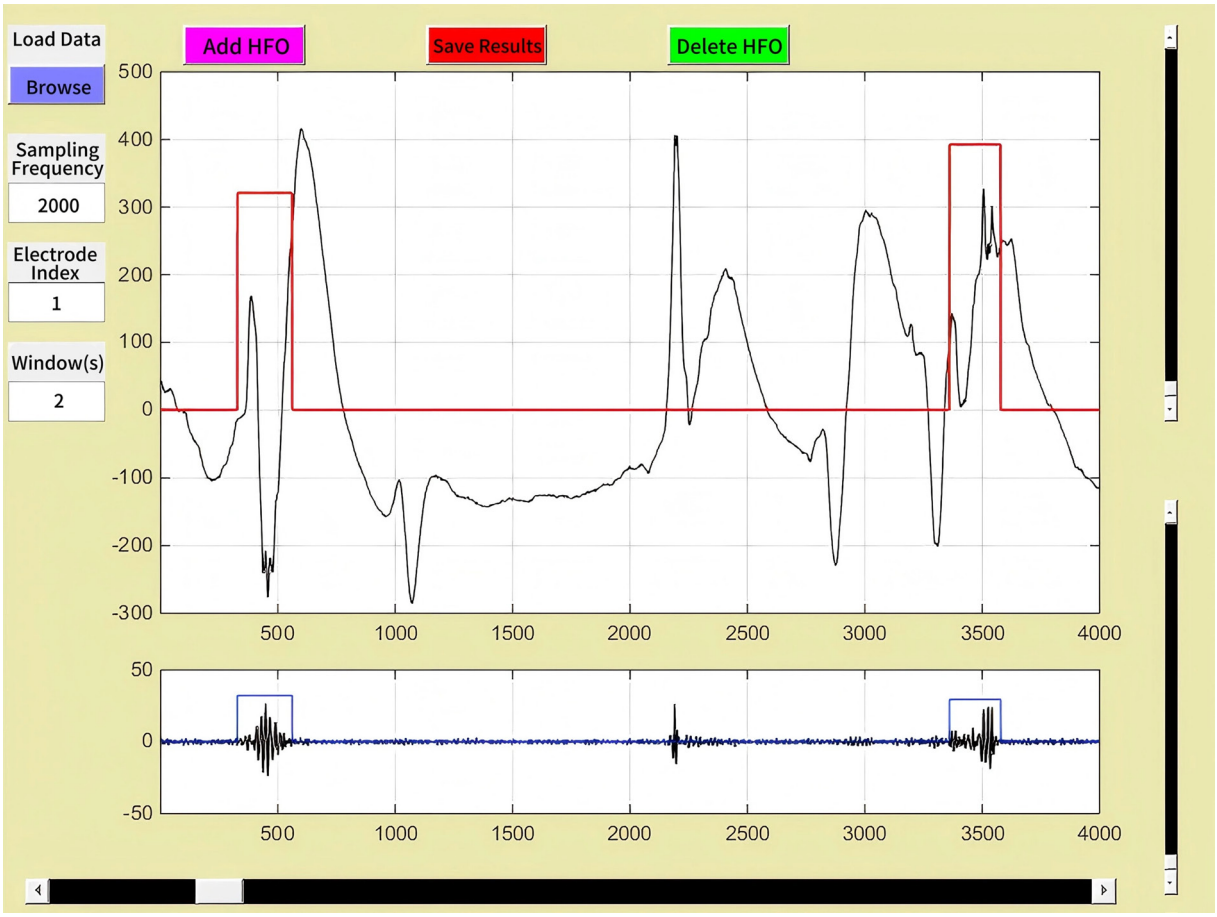

community for the quantitative evaluation of artifact denoising methods. Regarding the noise addition and mixing stages, we combined the 314 annotated pure raw iEEG signals with the EOG and EMG data segments from EEGdenoiseNet to generate artifact-contaminated EEG signals. This was achieved using a linear noising approach with SIR values ranging from −14 dB to 5 dB, as follows:

$$\mathrm{EEG}_{\mathrm{Contaminated}} = \mathrm{iEEG}_{\mathrm{Initial}} + \lambda^{*}\mathrm{Artifact}_{\mathrm{EOG\ or\ EMG}} \quad (1)$$

where λ is the artifact coefficient derived from the noise-added EEGs associated SIR. In our case, the following λ values were used: 3, 8, 12, 16, 20, 22, and 25. Both the initial iEEG signal and the artifact (EOG or EMG) were normalized prior to mixing. We then proceeded by randomly mixing the entire artifacts and actual iEEG data. The signal-to-interference ratio (SIR) computation method [21–22, 27, 28] was calculated as follows:

$$\mathrm{SIR}_{(\mathrm{dB})} = 10\log_{10}\left[\frac{\mathrm{RMS}(\mathrm{EEG}_{\mathrm{initial}})}{\mathrm{RMS}(\lambda^{*}\mathrm{Artifact}_{\mathrm{EOG\ or\ EMG}})}\right] \quad (2)$$

where RMS denotes the root mean square operator. Following these preprocessing stages, a total of 23,072 EMG and EOG-noised EEG signals covering SIR values between −14 dB and 5 dB were obtained. The contaminated EEG signals and raw iEEG samples were used as input and target output, respectively, to train the various DL models. 80% of the final preprocessed data were randomly selected and reserved for training, while the remaining 20% were evenly split between validation and testing, using 10-fold cross-validation.

2.3. DL denoising models: core architectures and hyperparameter tuning

In DL based applications, optimizing model performance hinges on several key hyperparameters. Some are commonly applicable across various architectures, while others are specific to particular methods. Understanding these hyperparameters is crucial, as their optimal values are often drawn from extensive trial-and-error tuning tests. The most significantly common hyperparameters include the learning rate, number of epochs, optimizer choice, early stopping criteria, batch size, and cost function. As one of the most critical hyperparameters, learning rate helps determine how quickly a model adapts during training by controlling weight updates. A recommended starting value is 0.0001, and the choice of a learning rate could significantly impact the model's overall performance. The number of epochs refers to the total passes performed through the training dataset, and setting up this parameter requires an equitable balance of underfitting and overfitting. When a model is underfitted, it fails to maintain effective learning, leading to poor performance at the levels of the training and validation datasets. Overfitting, however, occurs when a model appears to learn the training data perfectly well, which often results in excellent performance at the training set level, yet, poor generalization in regard to new latently implicit data. Hence, early stopping might help in mitigating overfitting by halting training when performance metrics stagnate, once a patience parameter is typically set between 3 and 25 epochs for regression tasks. More particularly, the training loss would steadily decline, while the validation loss would initially decrease prior to rising anew at the occurrence of the overfitting process. As to early stopping, it serves to halt training at the level where validation loss reaches its minimum. In this regard, batch size displays a noticeable impact on training dynamics, wherein, larger sizes could speed up training but might hinder generalization, while smaller sizes might enhance generalization at the expense of increased noise and execution time. The cost function, enabling to quantify the difference between predicted values and actual values, is vital for guiding the model learning process. Hence, the need to apply common loss metrics, with the most popular being the mean squared error (MSE) and the mean absolute error (MAE). Additionally, a wide range of optimizers were also applied to train DL models, including Stochastic Gradient Descent (SGD), RMSprop, and Adam, each distinctly influencing convergence and learning efficiency processes. Regarding hyperparameters, they were specifically tailored to meet each DL model special needs. Regarding the CNNs, for instance, multiple convolutional layers were applied for the features' extraction purposes, wherein, each layer uses different convolutional filters, followed by a max pooling process. Each layer was activated using Relu, and the network concludes with a fully connected layer, enclosing multiple hidden layers with N neurons. As regards the LSTMs, they were adept at capturing intricate temporal patterns within uni-dimensional data, such as time series, and were typically designed to use N LSTM units. Concerning SAEs, they apply a special encoder–decoder device to reflect learning representation modes, highly critical for deciphering complex data structures. The encoder compresses input data into a lower-dimensional latent space, capturing essential features, while the decoder undertakes to reconstruct the original input, allowing the model to estimate relevant effectiveness. Stacking multiple layers of encoders and decoders enhances the AEs' ability to learn hierarchical representations. Initially introduced in 2017, Transformers [36] represent powerful DL architectures fit for implementation in various applications, including the EEG signal analysis domains. Their built-in self-attention and multi-head attention mechanisms enable the model to weigh the importance of various input elements, by capturing dependencies within the same sequence and modeling relationships across different representation subspaces through attention mechanisms. Briefly, transformers encompass an embedded layer, enabling to convert input data into a meaningful vector space, while positional encoding adds sequential context order, enabling models to handle complex structured data with both relational and positional understanding, and a set of transformer–encoder data processing layers that apply attention-based techniques, along with a feed-forward layer or Multi-Layer Perceptron (MLP) as an extra transformation unit. Finally, the GANs, originally introduced by Goodfellow et al. [37], stand as a powerful DL modeling class, involving two neural networks: the generator and the discriminator. Actually, a GAN is a DL method based on two adversarial neural network architectures, a Discriminator (D) and a Generator (G), to produce highly realistic synthetic data. The Generator serves to generate new data samples from random noise inputs, aimed to mimic real data, while the Discriminator helps in ensuring whether the devised samples are genuine or generated. The G's major goal consists in producing data that D would mistakenly identify as real, leading to significant updates for G and penalties for D. Inversely, however, if D manages to correctly identify fake data, it turns out to be more adept at discrimination. This adversarial process iteratively refines both networks, enhancing the generator's ability to produce realistic synthetic data until the discriminator can no longer reliably distinguish between real and generated samples. Therefore, the objective function of a GAN can be expressed as a minimax optimization procedure, as described by the following equation:

$$\min_{\mathrm{G}}\max_{\mathrm{D}} \mathrm{V}(\mathrm{D},\mathrm{G}) = \mathrm{E}_{\mathrm{x}\sim pdata(x)}[\log(\mathrm{D}(\mathrm{x})] + \mathrm{E}_{\mathrm{z}\sim pz(z)}[\log(1-\mathrm{D}(\mathrm{G}(\mathrm{z})))] \quad (3)$$

Here, x denotes a sample drawn from the real data distribution $pdata(x)$, while $pz(z)$ represents the random input noise fed into the generator. D(x) corresponds to the discriminator's output for real data, while D(G(z)) corresponds to its output for generated data. G(z) is the generated (fake) sample produced from random noise z. For a comprehensive understanding of the provided GAN frameworks and their applications, the aforementioned-cited source [37] offers valuable in-depth analyses.

2.4. Performance evaluation metrics applied for EEG denoising regression tasks

Selecting the most appropriate evaluation metrics is crucial in the area of regression-based biomedical healthcare applications. In this context, we opted for adopting and implementing the previous studies' applied evaluation metrics, dealing with the subject of EEG denoising, consistently with their denoising performance assessment criteria. The aim was to elucidate each denoising model associated strength, to provide useful insights as to the most effective model selection process. In the process, each model's practical implications and limitations were outlined, paving the way for future innovations in matters of scalp EEG based HFO denoising procedure. For this purpose, five objective quantitative performance metrics were applied to evaluate and report the regression models' performance, while measuring error ranges between denoised EEG signals and true iEEG signals [23, 34]. In this respect, evaluating the different networks' performance was performed in terms of relative root mean square error in time ($RRMSE_t$), spectral relative root mean square error in frequency domain ($RRMSE_f$), along with the Pearson correlation coefficient values. In effect, both the temporal Pearson correlation coefficient (CC_t) and frequency Pearson correlation coefficient (CC_f) should help in pinpointing each method's ability to effectively preserve both temporal change and spectral information between the initial iEEG signals and denoised EEG signals. Additionally, time-frequency Pearson correlation coefficient (CC_{tf}) was also introduced to provide information regarding the method's ability to simultaneously preserve temporal and spectral information. The $RRMSE_t$ was used to measure the difference between the DL model predicted temporal EEG signal (y_i) and the ground truth time-series iEEG signal (x_i), as defined by:

$$\mathrm{RRMSE_t} = \sqrt{\frac{\sum (x_i - y_i)^2}{\sum (x_i)^2}} \tag{4}$$

On considering the frequency domain, the PSD was introduced to compute the $RRMSE_f$, as follows:

$$\mathrm{RRMSE_t} = \sqrt{\frac{\sum [PSD(x_i) - \mathrm{PSD}(y_i)]^2}{\sum \mathrm{PSD}\,(x_i)^2}} \tag{5}$$

wherein, the function PSD denotes the signal's power spectral density. The PSD frequency range in our case is 0–1000 Hz.

The correlation coefficient (CC), is the classic correlation measure of time-series data, also referred to as Pearson correlation coefficient. It serves to measure the degree of statistical relationship binding two variables, i.e., the ground truth signal and the denoised signal, in our case. The CC_t takes values within the range of [−1; 1], defined in time domain as:

$$\mathrm{CC_t} = \frac{\sum (x_i - \bar{x})(y_i - \bar{y})}{\sqrt{\sum (x_i - \bar{x})^2 \sum (y_i - \bar{y})^2}} \tag{6}$$

where: $\bar{x}$ and $\bar{y}$ respectively denote the average values of the iEEG ground truth and the DL model output. The fourth quantitative evaluative metric of our denoising model was determined by computing the correlation coefficient (CC) between both PSD of ground truth signal and denoised signal, defined as:

$$\mathrm{CC_f} = \frac{\sum \left(PSD(x_i) - \overline{PSDx}\right)\left(\mathrm{PSD}(y_i) - \overline{PSDy}\right)}{\sqrt{\sum \left(PSD(x_i) - \overline{PSDx}\right)^2 \sum \left(\mathrm{PSD}(y_i) - \overline{PSDy}\right)^2}} \tag{7}$$

where: $\overline{PSDx}$ and $\overline{PSDy}$ respectively designate the average values of the ground truth EEG signal spectrum and the model output spectrum. The final metric applied was the correlation between the time-frequency map of the true EEG signal and the denoised signal, denoted as CC_{tf}. In our study context, the Complex Morlet (CMOR) wavelet was applied to map time-frequency, as detailed in Chaibi et al. [38] (for further implementation details). This metric value was computed as follows:

$$\mathrm{CC_{tf}} = \frac{\mathrm{n}\sum(\mathrm{xy}) - \sum(\mathrm{x})\sum(\mathrm{y})}{\sqrt{\left[\mathrm{n}\sum \mathrm{x}^2 - (\sum \mathrm{x})^2\right]\left[\mathrm{n}\sum \mathrm{y}^2 - (\sum \mathrm{y})^2\right]}} \tag{8}$$

where: x and y respectively denote the time-frequency matrix maps within the 0–1000 frequency range of the original iEEG signal and the denoised signal, respectively, while n represents the flattened size of the TF map. In qualitative research, visual data analysis serves as a highly fruitful tool, enabling clearer interpretation of findings by transforming complex results into intuitive and accessible visual representations. Through radar charts, figures, and curves, it presents data in a reader-friendly format that improves comprehension and facilitates deeper insights.

3. Results

Most available DL algorithms trained on invasive EEG recordings perform poorly when applied to scalp EEG data, primarily due to the lower signal-to-interference ratios and the susceptibility of scalp EEG to various artifacts. These artifacts can mask persistent high-frequency phenomena. Moreover, different types of EEG artifacts and HFOs often exhibit similar morphological characteristics in both the time and frequency domains, potentially leading to misidentification of HFOs and adversely impacting clinical interpretations. To address these challenges, it is essential to evaluate the performance of these algorithms specifically for denoising scalp HFOs. This section focuses on tuning and optimizing both common and shared DL hyperparameters and their specific internal architectures, as their proper selection and adjustment are critical for enhancing models' performance in regression tasks like ours, ensuring stability, and improving generalization.

Table 1 presents the optimal shared hyperparameter values identified through extensive trial-and-error tuning, using both manual and Bayesian optimization methods. Various settings, including learning

Table 1
Optimal hyperparameters applied in the EEG denoising context

	Hyperparameter						
Method	**Optimizer**	**Loss function**	**Batch size**	**Number of epochs in early stopping**	**Learning rate**	**Cross-validation**	**Patience used in early stopping**
CNN-1D	RmsProp	MSE	25	391	0.00001	10-K-Folders	6
LSTM				371	0.00002		
Stacked AE				500	0.00005		
Transformer 1D				217	0.00002		
GAN				273	0.0008		

rates (ranging from 10^{-8} to 0.1), batch sizes (3 to 50), optimizers (SGD, Adam, RMSprop, Adadelta), and loss functions (MSE, MAE), were systematically evaluated to assess their impact. Different models were initially trained for 500 epochs, with early stopping applied to each architecture to prevent overfitting. Furthermore, k-fold cross-validation (k = 5 to 15) was iteratively tested through trial and error to determine the best trade-off between performance and computational cost.

Figure 3 provides an overview of the specifically optimized model configurations, along with the complete set of tuned architectures. Regarding the CNN method, we consistently employed three

Figure 3

Graphical illustrations of the various tuned DL architectures applied for HFO-sequence denoising: (a) CNN-1D, (b) LSTM, (c) stacked auto-encoder, (d) Transformer-1D and (e) GAN model architecture

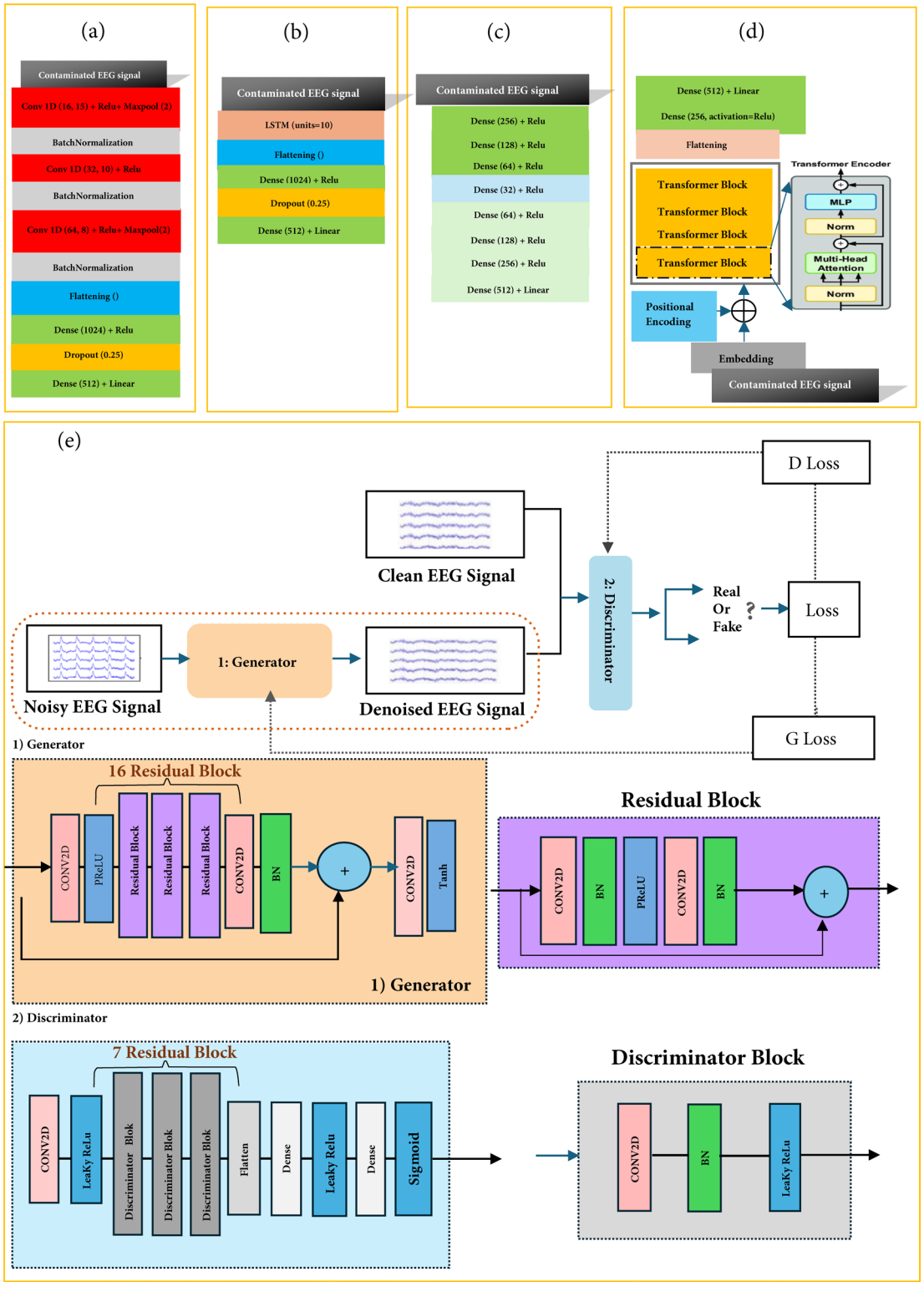

convolutional layers with kernel sizes of 15, 10, and 8, respectively, each activated by the ReLU function. Max pooling layers were applied after the first and third convolutional layers, while batch normalization followed all convolutional layers. For the fully connected module, two dense layers were used, separated by a dropout layer to reduce overfitting. The first dense layer contained 1024 neurons and utilized the ReLU activation function. The output dense layer comprised 512 neurons, corresponding to the denoised EEG signal, and applied a linear activation function suitable for regression tasks. With respect to the LSTM method, we employed ten units followed by a flattening of all resultant outputs. Subsequently, the same fully connected layers used in the CNN-1D model were applied to the LSTM model. The stacked autoencoder comprises an encoder, a bottleneck layer, and a decoder. The encoder has three ReLU-activated dense layers (256, 128, and 64 neurons), followed by a 32-neuron bottleneck layer for compressed feature extraction. The decoder mirrors this structure in reverse, ending with a linear activation layer of 512 neurons to reconstruct the denoised EEG signal. The temporal Transformer-based method begins with an embedding layer that converts raw contaminated EEG time series into dense vectors, capturing key features while reducing dimensionality. Positional encoding is applied to preserve the temporal order of data points. The model uses four transformer blocks (as configured in Vaswani et al. [36]), after which the output is flattened and passed through a MLP comprising two dense layers with 256 and 512 neurons. A linear activation function is applied at the output layer for continuous regression tasks like EEG denoising. The GAN architecture, shown in Figure 3, includes a Generator with 16 residual blocks and three 2D convolutional layers, ending with a Tanh activation for regression. The Discriminator consists of a convolutional layer followed by seven residual blocks and two dense layers; the first uses leaky ReLU activation, and the final layer applies a sigmoid activation to classify EEG signals as real or fake. Further implementation details and parameters are provided in Sawangjai et al. [29].

As summarized in Table 2, the performance evaluation and quantitative experimental results demonstrate the exceptional and superior reliability of the proposed GAN-based EEG denoising model. The model achieved excellent regression results, with time-domain $RRMSE_t$ and frequency-domain RRMSEf values of 0.0007 and 0.031, respectively. Additionally, the Pearson correlation coefficients were 0.995 for the time domain (CC_t) and 0.998 for the frequency domain (CC_f). The time–frequency metric (CC_{tf}) yielded a score value of 0.810.

Additionally, visualizing and comparing the loss trends across epochs for both training and validation sets provided valuable insights into the models' convergence behavior. As shown in Figure 4, the loss curves illustrate how the models evolved during training, enabling assessment of their learning trajectories and convergence toward optimal solutions. All models demonstrated good convergence and consistent improvement in generalizability throughout the training iterations. This visual comparison helps to understand and evaluate models' effectiveness, thereby supporting more effective fine-tuning and optimization.

Noteworthy as shown in Figure 4, the GAN model nearly converged to zero loss values, demonstrating markedly superior accuracy and effectiveness compared to the other DL models.

4. Discussion

While several DL algorithms exist for detecting HFOs in intracranial EEG, clinical applications often rely on scalp EEG due to its non-invasive nature and safety. Scalp EEG enables real-time and simple monitoring of brain activity but is frequently contaminated by artifacts such as EMG, EOG, and other noise, which can lead to spurious detections and inaccurate clinical interpretation of HFOs.

To address these challenges, this study introduced five DL methods designed to remove artifacts while preserving HFO features in scalp EEG signals. Accordingly, we examined several advanced DL denoising techniques, including CNN-1D, LSTM, Stacked Autoencoders, Transformer-1D, and GAN models. These five networks were designed to reduce EMG and EOG artifacts in contaminated EEG samples containing HFOs. Performance was evaluated using the Relative Root Mean Square Error (RRMSE) to quantify information retention and the Correlation Coefficient (CC) to assess similarity between the denoised and original signals across different domains. After tuning and evaluating these models, our goal was to identify the most effective method for denoising scalp EEG signals in the context of HFO processing. Figure 5 illustrates the strengths and weaknesses of each model. Notably, the GAN model demonstrated superior performance by minimizing total error ($RRMSE_t$ and $RRMSE_f$) while maximizing correlation coefficients (CC_t, CC_f, and CC_{tf}), outperforming the other DL methods in denoising HFO sequences.

For a qualitative analysis of different denoising models, Subplot 6(1,1) displays a contaminated EEG segment alongside the denoised signal produced by the CNN-1D model, as well as the corresponding true iEEG signal. Subplot 6(1,2) compares the power spectral density (PSD) of the CNN-1D denoised EEG with that of the original iEEG signal, while Subplots 6(1,3) and 6(1,4) show the spectrograms of the original and denoised signals, respectively, with time on the horizontal axis and frequencies from 0 to 1000 Hz on the vertical axis. This model failed to fully preserve the HFO representation observed in the original iEEG spectrogram. Graphs 6(2,1) through 6(2,4) present similar results for the LSTM method, which also failed to retain the HFO event information. Illustrations 6(3,1)–6(3,4) present results for the Stacked Autoencoder approach, which exhibited significantly poorer performance than the earlier models in retaining HFO-related information. For the Transformer-1D model, Subplots 6(4,1) through 6(4,4) illustrate outputs that inadequately preserve HFO burst traces across different domains. Finally, Graphs 6(5,1) through 6(5,4) present the GAN model results,

Table 2
Comparison of denoising performance of various DL networks

	Metric value				
Model	**$RRMSE_t$ temporal**	**$RRMSE_f$ spectral**	**CC_t temporal**	**CC_f spectral**	**CC_{TF} time-frequency**
CNN-1D	0.124	0.403	0.906	0.964	0.575
LSTM 1D	0.125	0.353	0.904	0.961	0.608
Stacked AE	0.138	0.235	0.890	0.954	0.676
Transformer-1D	0.172	0.645	0.809	0.922	0.655
GAN	0.0007	0.031	0.995	0.998	0.810

Note: Average values were reported across all SIR levels.

Figure 4
Depiction of training and validation loss curves of the compared DL models for HFOs segments denoising: (a) CNN-1D, (b) LSTM, (c) Stacked auto-encoder, (d) Transformer-1D and (e) GAN model architecture

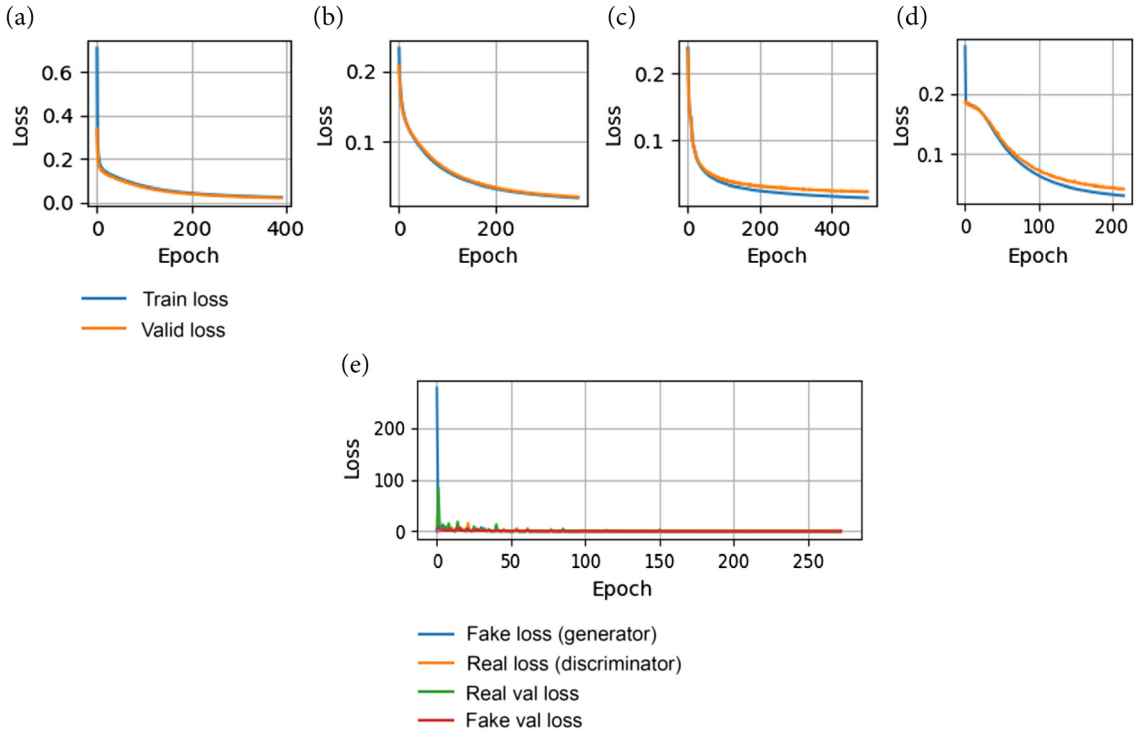

Figure 5
Radar chart-based performance evaluation of the selected EEG denoising regression networks

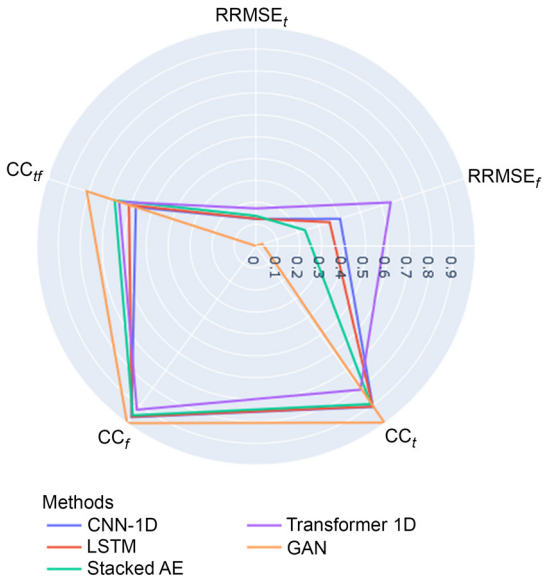

demonstrating its superior effectiveness in artifact removal. The GAN successfully preserved HFO traces in the denoised signal, which closely approximates the benchmark iEEG signal across time, frequency, and time–frequency domains.

Overall, the GAN model demonstrates strong performance compared to the other DL-based models, which exhibited limited accuracy in artifact denoising. This is reflected by correlation coefficients significantly below 1 (unity) and RRMSE values that remain notably above zero. Such limitations can result in inaccurate denoising of scalp HFO segments, particularly when processing signals containing overlapping transient artifacts (e.g., EMG or eye-blink artifacts) under low SIR conditions.

In summary, the proposed GAN model excels at denoising artifact-contaminated scalp EEG signals while preserving essential HFO features. Its effective noise reduction and accurate neural signal reconstruction make it a valuable tool for improving the reliability of HFO denoising in scalp EEG, thereby enhancing both clinical and research applications of HFOs.

This study acknowledges several limitations. First, although the GAN model demonstrated impressive results in denoising HFOs with as few as 314 labeled real HFO samples, its generalizability may be limited due to the small dataset size. A larger and more diverse dataset is necessary to capture the complex variations present in real-world HFO signals.

Second, internal validation was performed using data from a single institution. To improve the generalizability and clinical applicability of our findings, external validation using multi-center data representing a wide range of ages, symptoms, and clinical HFO profiles is essential. This would help further refine the GAN model and ensure its broader generalizability.

Third, no systematic comparison against conventional baseline methods and other machine learning approaches has been performed, hindering an objective assessment of progress in the field.

In conclusion, since our results are preliminary and not yet fully conclusive, large-scale multicenter validation studies are required to establish the reliability and generalizability of these findings prior to clinical application.

Figure 6
Qualitative comparison of EEG denoising models. Rows 1–5 correspond, respectively, to the CNN-1D, LSTM, Stacked Autoencoder, Transformer-1D, and GAN models

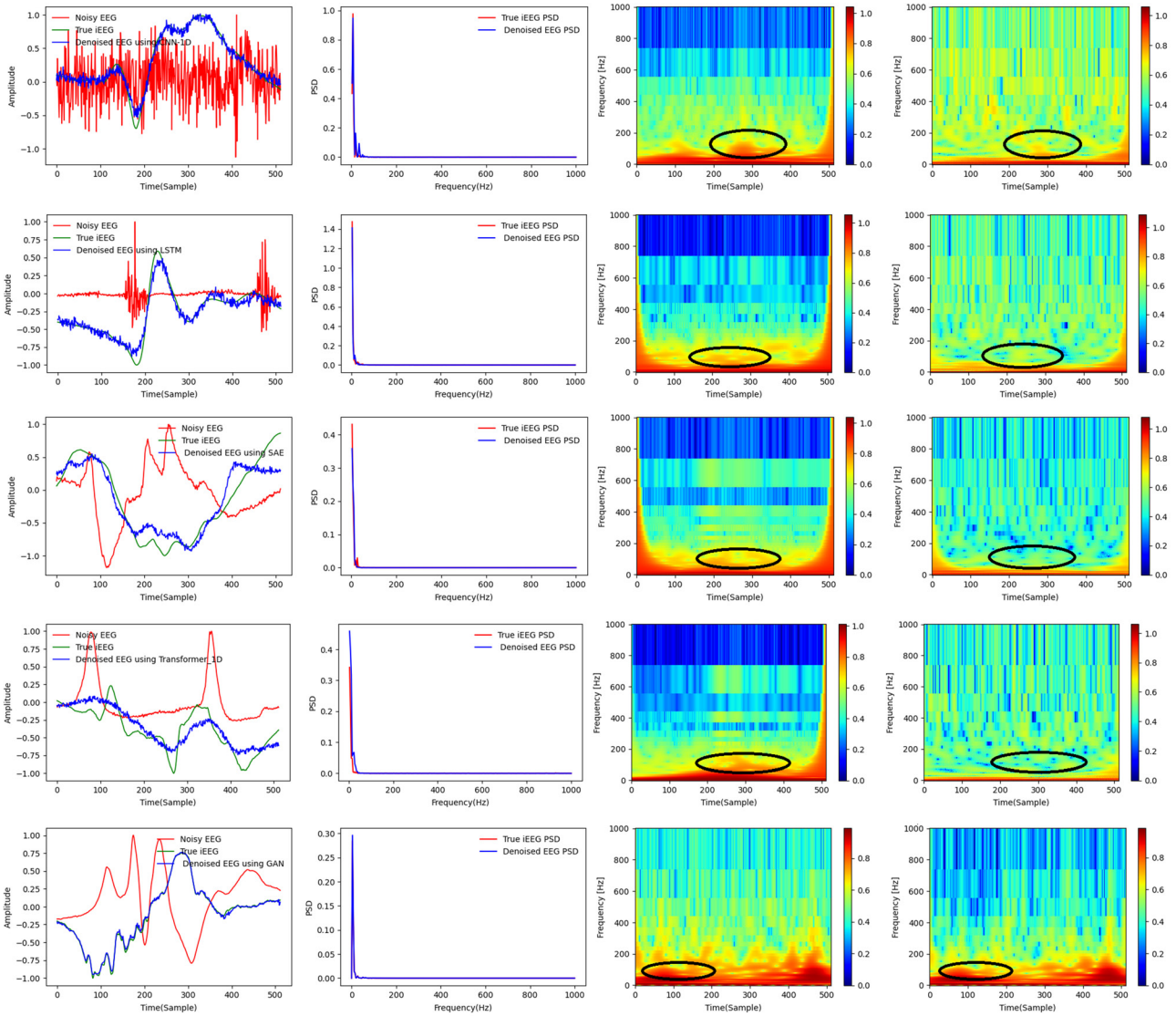

5. Conclusion and Future Research Veins

Accordingly, our present framework consisted of providing a systematic review and comparative analysis of five proposed EEG denoising fine-tuned DL models, using both the EEGdenoiseNet dataset and our own dataset as a consistent evaluative benchmark. In this regard, a set of five DL architectures, designed to remove EMG and EOG artifacts from contaminated EEG signals, was assessed by evaluating each model's robustness in this context. The reached findings clearly demonstrated the GAN model's high reliability in removing artifacts from contaminated EEG data, showing superior robustness across varying noise conditions and achieving strong performance in denoising HFO sequences in scalp EEG. Indeed, it achieved the lowest temporal and spectral relative root mean square errors (RRMSEs) of 0.0007 and 0.031, respectively, along with the highest temporal and spectral correlation coefficients of 0.995 and 0.998, respectively. Additionally, the time–frequency correlation coefficient (CC_{tf}) reached 0.810.

Ultimately, our approach may open new avenues by bridging the gap between invasive and non-invasive EEG processing, providing a clinically viable alternative for epilepsy cases where intracranial EEG is impractical or high-risk without requiring invasive procedures.

Potentially, our future research is likely to follow the following roadmap: (i) testing advanced DL models, such as large language models (LLMs) [39]; (ii) exploring additional evaluation metrics, including R-squared, mean absolute error (MAE), and median absolute error (MedAE); and (iii) collaborating with multiple institutions to assess the feasibility and generalizability of our findings using larger datasets, incorporating more intracranial HFO segments along with their corresponding scalp EEG data for validation [38, 40–42].

Acknowledgment

The authors gratefully acknowledge the staff at the Montreal Neurological Institute and Hospital in Canada for generously providing the dataset used in this study to evaluate various DL denoising models.

The authors would like to express their sincere gratitude to the members of the Functional Exploration of the Nervous System Service

at CHU Sahloul, Sousse, Tunisia, for their valuable assistance and professionalism in the visual inspection process of HFOs in our dataset.

We would also like to thank the editor and reviewers for their insightful comments and suggested recommendations relevant to the present manuscript.

Special thanks are also extended to Prof. Sami CHAMI, for his valuable assistance in matters of linguistic proofreading and structural review of the present manuscript.

Ethical Statement

The authors declare that all potential respondents were fully informed about the survey and participation was voluntary.

Conflicts of Interest

The authors declare that they have no conflicts of interest to this work.

Data Availability Statement

Data were available from the corresponding author upon reasonable request.

Author Contribution Statement

Sahbi Chaibi: Conceptualization, Methodology, Software, Validation, Formal analysis, Investigation, Resources, Data curation, Writing – original draft, Writing – review & editing, Visualization, Project administration. **Wadhah Ayadi:** Conceptualization, Methodology, Validation. **Abdennaceur Kachouri:** Validation, Supervision.

References

[1] Stovall, T., Hunt, B., Glynn, S., Stacey, W. C., & Gliske, S. V. (2021). Interictal high frequency background activity as a biomarker of epileptogenic tissue. *Brain Communications*, *3*(3), fcab188. https://doi.org/10.1093/braincomms/fcab188

[2] Lin, J., Smith, G. C., Gliske, S. V., Zochowski, M., Shedden, K., & Stacey, W. C. (2024). High frequency oscillation network dynamics predict outcome in non-palliative epilepsy surgery. *Brain Communications*, *6*(1), fcae032. https://doi.org/10.1093/braincomms/fcae032

[3] Zhang, Y., Chung, H., Ngo, J. P., Monsoor, T., Hussain, S. A., Matsumoto, J. H., ..., & Nariai, H. (2022). Characterizing physiological high-frequency oscillations using deep learning. *Journal of Neural Engineering*, *19*(6), 066027. https://doi.org/10.1088/1741-2552/aca4fa

[4] Guragain, H., Cimbalnik, J., Stead, M., Groppe, D. M., Berry, B. M., Kremen, V., ..., & Brinkmann, B. H. (2018). Spatial variation in high-frequency oscillation rates and amplitudes in intracranial EEG. *Neurology*, *90*(8), e639–e646. https://doi.org/10.1212/WNL.0000000000004998

[5] Fan, Y., Dong, L., Liu, X., Wang, H., & Liu, Y. (2021). Recent advances in the noninvasive detection of high-frequency oscillations in the human brain. *Reviews in the Neurosciences*, *32*(3), 305–321. https://doi.org/10.1515/revneuro-2020-0073

[6] Cserpan, D., Gennari, A., Gaito, L., Lo Biundo, S. P., Tuura, R., Sarnthein, J., & Ramantani, G. (2022). Scalp HFO rates are higher for larger lesions. *Epilepsia Open*, *7*(3), 496–503. https://doi.org/10.1002/epi4.12596

[7] Foley, E., Quitadamo, L. R., Walsh, A. R., Bill, P., Hillebrand, A., & Seri, S. (2021). MEG detection of high frequency oscillations and intracranial-EEG validation in pediatric epilepsy surgery. *Clinical Neurophysiology*, *132*(9), 2136–2145. https://doi.org/10.1016/j.clinph.2021.06.005

[8] Milon-Harnois, G. (2023). Détection automatique et analyse des oscillations à haute fréquence en EEG-HD de surface [Scalp HD-EEG high frequency oscillations automatic detection and analysis]. PhD Thesis, Université d'Angers.

[9] Jacobs J, Staba R, Asano E, Otsubo H, Wu JY, Zijlmans M, …, Gotman J. High-frequency oscillations (HFOs) in clinical epilepsy. *Prog Neurobiol*. (2012) Sep;98(3):302–15. http://doi.org/10.1016/j.pneurobio.2012.03.001

[10] Fazli Besheli, B., Sha, Z., Gavvala, J.R. et al. Using high-frequency oscillations from brief intraoperative neural recordings to predict the seizure onset zone. *Commun Med 4*, *243* (2024). https://doi.org/10.1038/s43856-024-00654-0

[11] Wang, Z., Guo, J., van'T Klooster, M., Hoogteijling, S., Jacobs, J., & Zijlmans, M. (2024). Prognostic value of complete resection of the high-frequency oscillation area in intracranial EEG: A systematic review and meta-analysis. *Neurology*, *102*(9), e209216. https://doi.org/10.1212/WNL.0000000000209216

[12] Sun, Y., Ren, G., Ren, J., & Wang, Q. (2021). High-frequency oscillations detected by electroencephalography as biomarkers to evaluate treatment outcome, mirror pathological severity and predict susceptibility to epilepsy. *Acta Epileptologica*, *3*(1), 29. https://doi.org/10.1186/s42494-021-00063-z

[13] Fedele, T., van'T Klooster, M., Burnos, S., Zweiphenning, W., van Klink, N., Leijten, F., ..., & Sarnthein, J. (2016). Automatic detection of high frequency oscillations during epilepsy surgery predicts seizure outcome. *Clinical Neurophysiology*, *127*(9), 3066–3074. https://doi.org/10.1016/j.clinph.2016.06.009

[14] Liu, J., Sun, S., Liu, Y., Guo, J., Li, H., Gao, Y., ..., & Xiang, J. (2020). A novel MEGNet for classification of high-frequency oscillations in magnetoencephalography of epileptic patients. *Complexity*, *2020*(1), 9237808. https://doi.org/10.1155/2020/9237808

[15] Zhang, X. (2024). Deep learning-based techniques for electroencephalogram (EEG) signal denoising. *Transactions on Computer Science and Intelligent Systems Research*, *5*, 922–927. https://doi.org/10.62051/rrve8560

[16] Höller, P., Trinka, E., & Höller, Y. (2018). High-frequency oscillations in the scalp electroencephalogram: Mission impossible without computational intelligence. *Computational Intelligence and Neuroscience*, *2018*(1), 1638097. https://doi.org/10.1155/2018/1638097

[17] Milon-Harnois, G., Jrad, N., Schang, D., van Bogaert, P., & Chauvet, P. (2022). Deep learning for scalp high frequency oscillations identification. In *2022 30th European Signal Processing Conference*, 1223–1227. https://doi.org/10.23919/EUSIPCO55093.2022.9909978

[18] Besio, W. G., Martinez-Juarez, I. E., Makeyev, O., Gaitanis, J. N., Blum, A. S., Fisher, R. S., & Medvedev, A. V. (2014). High-frequency oscillations recorded on the scalp of patients with epilepsy using tripolar concentric ring electrodes. *IEEE Journal of Translational Engineering in Health and Medicine*, *2*, 2000111. https://doi.org/10.1109/JTEHM.2014.2332994

[19] Chaibi, S., Mahjoub, C., Le Bouquin Jeannès, R., & Kachouri, A. (2023). Interactive interface for spatio-temporal mapping of epileptic human brain using characteristics of high frequency oscillations (HFOs). *Biomedical Signal Processing and Control*, *85*, 105041. https://doi.org/10.1016/j.bspc.2023.105041

[20] Ren, S., Gliske, S. V., Brang, D., & Stacey, W. C. (2019). Redaction of false high frequency oscillations due to muscle artifact improves specificity to epileptic tissue. *Clinical Neurophysiology*, *130*(6), 976–985. https://doi.org/10.1016/j.clinph.2019.03.028

[21] Chowdhury, M. E. H., Hossain, M. S., Mahmud, S., & Khandakar, A. (2022). Deep learning technique to denoise electromyogram artifacts from single-channel electroencephalogram signals. In *CS & IT Conference Proceedings*, 85–98. https://doi.org/10.5121/csit.2022.122006

[22] Huang, T.-Q., Wang, C.-S., Chen, Z.-Q., Zhang, F.-Q., Meng, X.-L., Grau, A., ..., & Huang, J.-W. (2023). 2-D GCANet applied to denoise 1-D EEG signals in online remote teaching scenarios. *Journal of Network Intelligence*, *8*(4), 1289–1302.

[23] Xiong, J., Meng, X.-L., Chen, Z.-Q., Zhang, F.-Q., Grau, A., Chen, Y., & Huang, J.-W. (2024). One-dimensional EEG artifact removal network based on convolutional neural networks. *Journal of Network Intelligence*, *9*(1), 142–159.

[24] Bekele, M. W., Eyob Abera, D., Hailemichael, M. T., Yeabsra Dechasa, K., Fanos, M. N., & Yared Getachew, M. (2023). Electroencephalography data denoising with deep neural networks. In *2023 IEEE International Conference on Control, Electronics and Computer Technology*, 1074–1078. https://doi.org/10.1109/ICCECT57938.2023.10140786

[25] Arsene, C. T. C., Hankins, R., & Yin, H. (2019). Deep learning models for denoising ECG signals. In *2019 27th European Signal Processing Conference*, 1–5. https://doi.org/10.23919/EUSIPCO.2019.8902833

[26] An, Y., Lam, H. K., & Ling, S. H. (2022). Auto-denoising for EEG signals using generative adversarial network. *Sensors*, *22*(5), 1750. https://doi.org/10.3390/s22051750

[27] Brophy, E., Redmond, P., Fleury, A., de Vos, M., Boylan, G., & Ward, T. (2022). Denoising EEG signals for real-world BCI applications using GANs. *Frontiers in Neuroergonomics*, *2*, 805573. https://doi.org/10.3389/fnrgo.2021.805573

[28] Dong, Y., Tang, X., Li, Q., Wang, Y., Jiang, N., Tian, L., ..., & Fang, P. (2023). An approach for EEG denoising based on wasserstein generative adversarial network. *IEEE Transactions on Neural Systems and Rehabilitation Engineering*, *31*, 3524–3534. https://doi.org/10.1109/TNSRE.2023.3309815

[29] Sawangjai, P., Trakulruangroj, M., Boonnag, C., Piriyajitakonkij, M., Tripathy, R. K., Sudhawiyangkul, T., & Wilaiprasitporn, T. (2022). EEGANet: Removal of ocular artifacts from the EEG signal using generative adversarial networks. *IEEE Journal of Biomedical and Health Informatics*, *26*(10), 4913–4924. https://doi.org/10.1109/JBHI.2021.3131104

[30] Wang, S., Luo, Y., & Shen, H. (2022). An improved Generative Adversarial Network for Denoising EEG signals of brain-computer interface systems. In *2022 China Automation Congress*, 6498–6502. https://doi.org/10.1109/CAC57257.2022.10055145

[31] Wang, Y., Luo, S., Ma, L., & Huang, M. (2023). RCA-GAN: An improved image denoising algorithm based on generative adversarial networks. *Electronics*, *12*(22), 4595. https://doi.org/10.3390/electronics12224595

[32] Jin, Y., Liu, A., Li, C., Qian, R., & Chen, X. (2023). Jīyú bìngxíng CNN hé Transformer de nǎo diàn jiàng zào wǎngluò [A parallel CNN and transformer network for EEG denoising]. *Journal of Signal Processing*, *39*(8), 1419–1432. https://dx.doi.org/10.16798/j.issn.1003-0530.2023.08.008

[33] Chen, J., Pi, D., Jiang, X., Xu, Y., Chen, Y., & Wang, X. (2024). Denosieformer: A transformer-based approach for single-channel EEG artifact removal. *IEEE Transactions on Instrumentation and Measurement*, *73*, 1–16. https://doi.org/10.1109/TIM.2023.3341114

[34] Leite, N. M. N., Pereira, E. T., Gurjao, E. C., & Veloso, L. R. (2018). Deep convolutional autoencoder for EEG noise filtering. In *2018 IEEE International Conference on Bioinformatics and Biomedicine*, 2605–2612. https://doi.org/10.1109/BIBM.2018.8621080

[35] Zhang, H., Zhao, M., Wei, C., Mantini, D., Li, Z., & Liu, Q. (2021). EEGdenoiseNet: A benchmark dataset for deep learning solutions of EEG denoising. *Journal of Neural Engineering*, *18*(5), 056057. https://doi.org/10.1088/1741-2552/ac2bf8

[36] Vaswani, A., Shazeer, N., Parmar, N., Uszkoreit, J., Jones, L., Gomez, A. N., ..., & Polosukhin, I. (2017). Attention is all you need. In *Proceedings of the 31st International Conference on Neural Information Processing Systems*, 6000–6010.

[37] Goodfellow, I. J., Pouget-Abadie, J., Mirza, M., Xu, B., Warde-Farley, D., Ozair, S., ..., & Bengio, Y. (2014). Generative adversarial nets. In *Proceedings of the 28th International Conference on Neural Information Processing Systems*, *2*, 2672–2680.

[38] Chaibi, S., Lajnef, T., Sakka, Z., Samet, M., & Kachouri, A. (2013). A comparison of methods for detection of high frequency oscillations (HFOs) in human intacerberal EEG recordings. *American Journal of Signal Processing*, *3*(2), 25–34.

[39] Vacareanu, R., Negru, V.-A., Suciu, V., & Surdeanu, M. (2024). From words to numbers: Your large language model is secretly a capable regressor when given in-context examples. *arXiv Preprint: 2404.07544*. https://doi.org/10.48550/arXiv.2404.07544

[40] Koessler, L. (2023). What are the advantages and challenges of simultaneous scalp EEG and intracranial EEG data recording? In N. Axmacher (Ed.), *Intracranial EEG: A guide for cognitive neuroscientists* (pp. 179–197). Springer. https://doi.org/10.1007/978-3-031-20910-9_12

[41] Wong, S. M., Sharma, R., Abushama, A., Ochi, A., Otsubo, H., & Ibrahim, G. M. (2024). The impact of simultaneous intracranial recordings on scalp EEG: A finite element analysis. Journal of Neuroscience Methods, 405, 110101. https://doi.org/10.1016/j.jneumeth.2024.110101

[42] Parmigiani, S., Mikulan, E., Russo, S., Sarasso, S., Zauli, F. M., Rubino, A., ..., & Pigorini, A. (2022). Simultaneous stereo-EEG and high-density scalp EEG recordings to study the effects of intracerebral stimulation parameters. *Brain Stimulation*, *15*(3), 664–675. https://doi.org/10.1016/j.brs.2022.04.007

How to Cite: Chaibi, S., Ayadi, W., & Kachouri, A. (2025). Effective Denoising of Epileptic High-Frequency Oscillations (HFOs) in Scalp EEG Using a Temporal Generative Adversarial Network (TimeGAN). *Artificial Intelligence and Applications*. https://doi.org/10.47852/bonviewAIA52025860